Detecting Small Targets With a Terahertz Radar

1st Karl L. Strecker School of Elec. & Comp. Engin. Oklahoma State University Stillwater, OK USA karl.l.strecker@okstate.edu

4rd Rajind Mendis *Riverside Research* Beavercreek, OH USA rmendis@riversidereseasrch.org 2th G. Levi Captain School of Elec. & Comp. Engin. Oklahoma State University Stillwater, OK USA george.captain@okstate.edu

5th John F. O'Hara School of Elec. & Comp. Engin. Oklahoma State University Stillwater, OK USA oharaj@okstate.edu 3nd Forrest Tuschhoff School of Elec. & Comp. Engin. Oklahoma State University Stillwater, OK USA ftuschh@okstate.edu

Abstract—This paper explores the application of terahertz radio detection and ranging (radar) systems for the detection and identification of small, low-RCS targets, specifically focusing on unmanned aerial vehicles such as drones. Traditional sensor systems often struggle with such targets due to their low radar cross-sections and the presence of environmental obstructions such as smoke, dust and fog. This study features experimental results from a 130 GHz radar system, which successfully demonstrated centimeter resolution and high-ranging accuracy against realistically low RCS targets. The results showed that current sub-terahertz technology could detect small drones at distances up to 300 m, with the potential to extend this range through longer observation times and higher carrier frequencies. The findings indicate that terahertz radar systems can provide reliable detection of challenging targets in unfavorable environments, filling a crucial technology gap by augmenting or replacing existing inadequate detection technologies.

Index Terms—millimeter-wave, terahertz, radar, drone, detection, RCS

I. INTRODUCTION

The detection of small and/or fast-moving objects presents a significant challenge to existing sensor systems [1]. A particular target class of interest is small multi-rotor "drones", which are widely available, inexpensive, and easy to operate. Unfortunately, these craft are also challenging to detect, and their versatility and low cost make multi-rotors useful to bad actors, who use them to carry explosives, infectious biological agents, drugs, and for illicit surveillance. For the same reasons, multi-rotors are also increasingly a significant part of modern wars, making reliable and timely detection of such craft a priority for security purposes.

Multi-rotors are particularly challenging to detect due to their compact design and low-altitude flight patterns. These drones often have a low radar cross-section (RCS), especially when constructed from non-metallic materials, thus can eas-

Funding support: This work was supported in part by the National Aeronautics and Space Administration, Grant 80NSSC22K0878, and the National Science Foundation, Grant ECCS-2238132.

ily blend into cluttered environments or be mistaken for birds by target-identification algorithms.

Wireless communications, infrared (IR) and visible light [2], and existing radar systems have all been used for drone tracking with differing levels of success, but all fall short of providing reliable detection in all scenarios. Fully autonomous drones that "fly dark" cannot be detected by communication-tracking systems, IR and visible light detection systems are easily obstructed by fog, dust, and smoke, and traditional radar systems tend to treat small, low-RCS targets as point scatterers (if they detect them at all), limiting the amount of information that can be gleaned from the reflected signals. As a result, there is a pressing need for the development of advanced sensor systems that can overcome these limitations and provide reliable detection of small, fast, low-RCS targets.

Terahertz frequencies (defined here as frequencies between 0.1 THz and 10 THz) possess the unique ability to penetrate through environmental obstructions such as smoke, fog, and dust [3]–[5], yet enable quasi-optical imaging. The fine spatial resolution achieved by terahertz radars allows for detailed imaging of objects, making them suitable for machine learning algorithms designed for target identification and classification [6], [7]. These algorithms can also analyze the rich micro-Doppler signatures available at terahertz frequencies to further distinguish between different drone types based on their unique signatures [8], or to distinguish them from other targets, such as birds [9]. This dual capability—penetrating environmental obstructions while providing high-resolution imaging and having returns rich in micro-Doppler signatures—makes terahertz radars an attractive solution for reliable unmanned aircraft systems (UAS) detection and identification in adverse conditions.

Terahertz systems are also attractive for drone detection because the RCS of aerial platforms (and targets in general) increases with electromagnetic frequency, due to increased diffuse scattering [7]. A study on the RCS signatures of diverse drone models found that the RCS of small to midsized rotorcraft fell between -15 dBsm and -6 dBsm at 40 GHz, and increased by approximately 0.25 dB/GHz over the 26-40 GHz band [10]. (The units of dBsm refer to decibel over square meter, that is, RCS decibels calculated with normalization to a RCS of one square meter.) Extrapolating this trend gives an RCS estimate of 7.5 dBsm to 16.5 dBsm for small and mid-sized rotorcraft at 130 GHz.

Similarly, a separate RCS analysis of a DJI Phantom 3 drone also found that its RCS increased with frequency, albeit at a lower rate of approximately 0.16 dB/GHz [11]. Extrapolating with this less-optimistic (and less general) estimate, the mean RCS of this drone is still predicted to be approximately 4 dBsm, which is higher than the smallest corner reflector used in our radar campaign. This substantial increase in RCS at higher frequencies suggests that terahertz radars can achieve reliable detection of drones (and other low RCS targets) at multi-kilometer ranges, making them a powerful tool for detecting such targets.

In this work, we demonstrate medium-range experimental results that confirm sub-centimeter resolution and high ranging accuracy in a terahertz radar system. Our experiments successfully detect corner reflectors with radar cross-sections commensurate with those of small drones, validating the system's effectiveness in detecting low-RCS targets. These promising results suggest that even current terahertz technology is sufficiently mature to successfully detect low RCS targets at useful ranges. Furthermore, terahertz systems employing slower sweep rates and/or enhanced coherent integration have the potential to detect, identify, and even image low-RCS objects such as drones at distances spanning multiple kilometers. This sets the stage for more effective and reliable long-range detection of challenging targets.

II. EXPERIMENTAL SETUP

Our experiments were performed July 2nd and 3rd, 2024, over a brick and concrete walkway at Oklahoma State University. This walkway is shown in Fig. 1(A) and (B). This thoroughfare was largely devoid of foot traffic during the summer break, and the location of power outlets along the walkway allowed us to set up radar equipment and targets separated by up to 341.4 meters. During the experiments, the average temperature varied between 31-34 °C (304-307 K).

For this experiment, the TWISTER system - a wideband millimeter-and-submillimeter-wave testbed composed of state-of-the-art commercial test instrumentation - was configured to act as a dual-sweep frequency modulated continuous wave (FMCW) radar. The TWISTER system is described in detail in our previous work [12], and is based around a Keysight M8195A arbitrary waveform generator (AWG), a collection of Virginia Diodes "compact converter" (CC) up/down conversion modules [13], a pair of Keysight E8257D analog signal generators, synchronized by a precision 1 GHz reference, that serve as local oscillators (LOs),





Fig. 1. In sub-figure (A), the target is located within the red circle, and the location of the radar is indicated by the white cross. Sub-figure(B) shows the view downrange from the nearly co-located transmitter (left dish) and receiver (right dish). A corner reflector, mounted on the radar-absorbing-material-covered tripod, is not visible in the distance, 341.4 meters away.

and a Keysight DSOV254A digital storage oscilloscope (DSO).

In all experiments, the TWISTER system was set up as an FMCW radar centered at 130 GHz, with a bandwidth of 5 GHz. The FMCW signal was dual-swept over $5\,\mu s$, meaning it swept from 127.5 GHz to 132.5 GHz for the first 2.5 μs , then from 132.5 GHz to 127.5 GHz for the second 2.5 μs , repeating this cycle every 5 μs . In all cases, the system operated in a quasi-monostatic configuration, with the nearly co-located receiver and transmitter separated by approximately 0.6 meters. A picture of the experiment and the TWISTER radar system is shown in Fig. 1.

During the first suite of measurements, trihedrial corner reflectors (TCRs) [14] of differing sizes were illuminated by the radar at ranges of 48.2 m, 96.6 m, 139.0 m, 192.6 m, 269.7 m, and 341.4 m. Table I gives details regarding the TCRs used. It is worth noting that the two smallest TCRs (shown in Fig. 2(A)) make particularly interesting targets, as their RCS values (-1.3 dBsm and 14.6 dBsm) roughly match the range of RCS values expected for small multirotor aircraft as calculated by extrapolating the results of [10], [11], up to 130 GHz (i.e., 4.0 dBsm to 16.5 dBsm).

During the second suite of measurements, a pair of flat rectangular mirrors with adjustable range separation (Fig. 2(B)) were set up at 192.6 m. The spacing of the mirrors was swept between 0 and 18 cm to test the range resolution

TABLE I
TETRAHEDRAL CORNER REFLECTORS (TCRS) USED AS TARGETS, THEIR
DIMENSIONS, PLATE GEOMETRY, AND PEAK RCS.

Target No.	Interior Edge Length	Geometry	RCS (dBsm)
TCR #1	43.2 cm	Triangular	44.34
TCR #2	8.0 cm	Square	24.63
TCR #3	4.5 cm	Square	14.63
TCR #4	1.8 cm	Square	-1.28

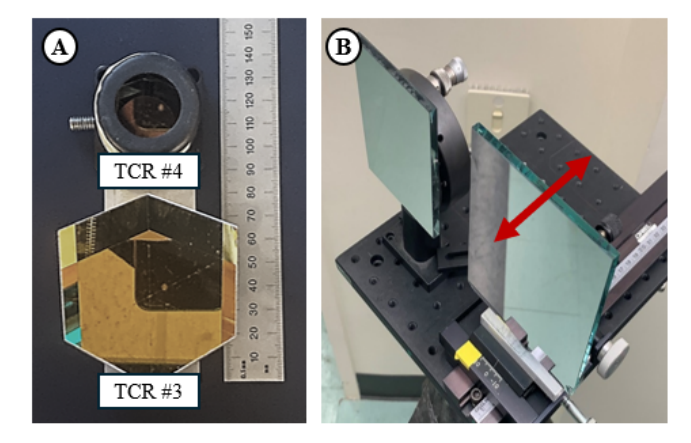


Fig. 2. Pictures of (A) the two smallest trihedrial corner reflectors used in the first suite of measurements, and (B) the flat mirrors with adjustable separation used in the range resolution test. The two TCRs shown in (A) have RCSs commensurate with those of small drones.

of the radar system.

III. THEORETICAL ANALYSIS

The average power emitted by the transmitter feedhorn was measured to be $P_{\rm tx}=25.2~{\rm mW}$ using a calorimeter-type power meter. During propagation, the transmitted power will spread out over the surface area of a sphere, and becomes an area power density $D_{\rm target}=GP_{\rm tx}/(4\pi R^2)$, where G is the gain of the transmitting antenna, and R is the range to the target. Both receiver and transmitter utilized Cassegrain-style dish antennas with a diameter of 0.305 m (1 ft) and an aperture efficiency of 0.4, which results in a gain of about 48 dB at 130 GHz. Thus, the target will be illuminated by an incident power density of $D_{\rm target}=138.19/R^2~{\rm W/m}^2$.

The amount of power re-radiated by the target depends on many factors, which are abstracted by modeling the target as an isotropic scatterer with a RCS of $\sigma_{\rm dB}$. The area power density of the return signal will thus be $D_{\rm scatter} = \sigma D_{\rm target}/(4\pi R^2)$, or, $D_{\rm scatter} = 11\sigma/(R^4)$ W, where $\sigma_{\rm dB} = 10\log_{10}\sigma$. For our smallest corner reflector with $\sigma_{\rm dB} = -1.28$ dBsm, the return area power density will be 8.18 W/m².

However, this area power density will be decreased somewhat by the fact that the TCRs used as targets direct the peak of the return toward the transmitter, resulting in a slight loss when operating in a *quasi*-monostatic configuration. This was measured and and modeled as a static 1.86 dB reduction in received area power density, but this number will vary with the size of the TCR and the range, and may represent a minimum measured value.

Finally, the power captured by the receiver will be $P_{\rm cap} = D_{\rm scatter} A_{\rm eff}$, where $A_{\rm eff}$ is the effective area of the antenna, defined as $A_{\rm eff} = G \lambda^2/(4\pi)$, where λ is the wavelength (2.3 mm at 130 GHz). In total, the return power for our system should be $P_{\rm ret} = \sigma 209.2/R^4$ mW, where R is measured in meters.

However, this estimate does not account for atmospheric attenuation, which may be significant at terahertz frequencies and affects the signal both on the outbound and return paths. During our experiment the temperature averaged 33 °C and the relative humidity was 50%; under these conditions, the atmospheric attenuation was approximately 2.5 dB/km. Thus, the anticipated receive power is decreased by a factor of 1.00115^R , so that $P_{\rm ret} = \sigma 209.2/(1.00115^R R^4)$ mW.

Upon entering the receiver's feedhorn, the signal is coupled into the compact downconversion (CCD) module. At our operating frequency, the CCD has a conversion loss of 11 dB. This is followed by an integrated IF amplifier with a gain of 12 dB, and an intermediate wideband amplifier with a gain of 30 dB, before the signal finally arrives at the analog-to-digital converter (ADC) of the oscilloscope. This results in a digitized signal power of $\sigma 263.35/(1.00115^R R^4)$ W.

Meanwhile, the thermal noise power at the entrance to the receiver feedhorn will be $P_n = \Delta f_n k_B T$ Watts, where k_B is the Boltzman constant, the temperature T is in degrees Kelvin, and noise bandwidth Δf_n is in Hertz. The noise bandwidth is a key parameter that, if handled incorrectly, will produce highly inaccurate estimates of the noise power. The noise bandwidth is not the swept bandwidth, but is the resolution bandwidth of the signal's Fourier transform. This is inversely proportional to the time the radar observes the target as a fundamental consequence of time-frequency duality. Consequently, for an FMCW radar with a sweep rate of $2.5\,\mu\rm s$, the noise bandwidth is 400 kHz, yielding a base thermal noise power of $1.684\,\rm fW$.

This thermal noise floor is unaffected by the 11 dB conversion loss in the mixer, but will be amplified by both the 12 dB integrated IF amplifier and the 30 dB wideband amplifier. Furthermore, additional noise will be injected by both amplifiers, which have noise figures of 13 dB and 14 dB respectively, and by the oscilloscope, which has a noise figure of 30 dB. As a whole, the receive chain has a noise figure of 13.34 dB, and a gain of 42 dB, which results in a digitized noise power of 577 pW.

Dividing the signal power by the noise power yields the signal-to-noise ratio (SNR) of the return under optimal (i.e., matched filter) processing. Using the values calculated so far, the expected SNR of the processed return is $\mathrm{SNR} = (\sigma/(1.00115^RR^4)) \cdot 4.58 \times 10^{11},$ or, in more convenient logarithmic units, $\mathrm{SNR} = 116.6 - 10\log_{10}\left(R^4\right) - 0.0025 \cdot (2R) + 10\log_{10}\left(\sigma\right) \, \mathrm{dB}.$

To conclude our analysis of the predicted performance of the TWISTER radar system, a few salient points bear mentioning. First, the observed SNR of the processed returns will never exceed 54 dB. This is because the Keysight M8195A AWG we used as a signal source has an 8-bit resolution, thus, digitization noise in the source signal limits the overall SNR to somewhat less than 54 dB. Second, the range resolution of the system, δR , depends on the sweep bandwidth according to $\delta R = c_0/(2\Delta f)$. For our system, which has a sweep bandwidth of 5 GHz, the range resolution is predicted to be 30 mm. Though the range *accuracy* can be more precise than this, adjacent targets separated in range by less than 30 mm will not be distinguishable and will appear as a single target [15].

IV. RESULTS

The return signals at 130 GHz were mixed to an intermediate frequency (IF) of 7.3 GHz, digitized by the DSO at a sample rate of 40 gigasamples per second, saved to file, and processed offline using MATLAB.

The measured returns for the four TCRs are tabulated in Table II. As expected, the return SNR is limited to less than 54 dB, saturating at approximately 48.5 dB due to the additional noise sources within the transmitter architecture. The return from the largest corner reflector, possessing a RCS of 44.3 dBsm, was so strong that the dynamic range limit was imposed by the transmitter at every distance. The returns from all targets exceeded the nominal 15 dB detection threshold at every distance measured. The two smallest TCRs were excluded from the 341.4 meter measurements, accordingly, and those table entries are labeled "NA".

TABLE II A TABLE SHOWING THE SNR OF THE PROCESSED RADAR RETURNS VERSUS RANGE AND TARGET RCS.

Range		Target Detection (SNR)				
		Corner Reflector RCS				
feet	meters	44.3 dBsm	24.6 dBsm	14.6 dBsm	-1.3 dBsm	
158	48.2	48.5	48.4	48.3	47.4	
317	96.6	48.3	48.4	48.3	41.9	
456	139.0	48.2	48.4	47.6	39.3	
632	192.6	48.9	45.0	38.1	21.5	
885	269.7	48.2	42.1	33.0	17.4	
1120	341.4	48.3	32.5	NA	NA	

These SNR values compare favorably with those predicted by theory. Fig. 3 shows theoretical curves versus experimental data for the three smallest RCS targets (the largest target is not shown because it consistently hit the 48.5 dB dynamic range limit). These demonstrate that our measured returns are very near those predicted by theoretical analysis. Interestingly, two of the measured data points for the -1.28 dBsm TCR target are significantly higher than theoretical predictions. We hypothesize this to be caused by cross-talk between the transmitter and receiver; during the experimental campaign, some leakage signal was discovered between the waveguide amplifiers in the transmitter's feed and the nearby receiver, producing spurious returns. During later measurements these were reduced by adding shielding, and in most measurements the spurious "targets" were easily identifiable. However, we currently hypothesize that in the anomalously high returns observed for the $-1.29~\mathrm{dBsm}$ target, the true return happened to overlap with one of the interfering signals, producing erroneously high signal powers.

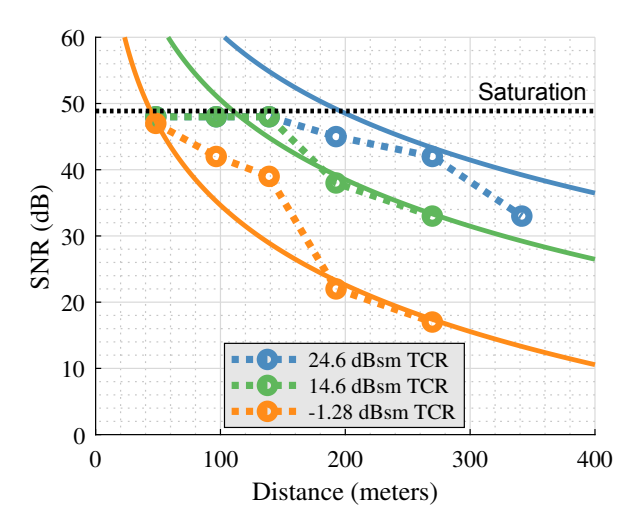
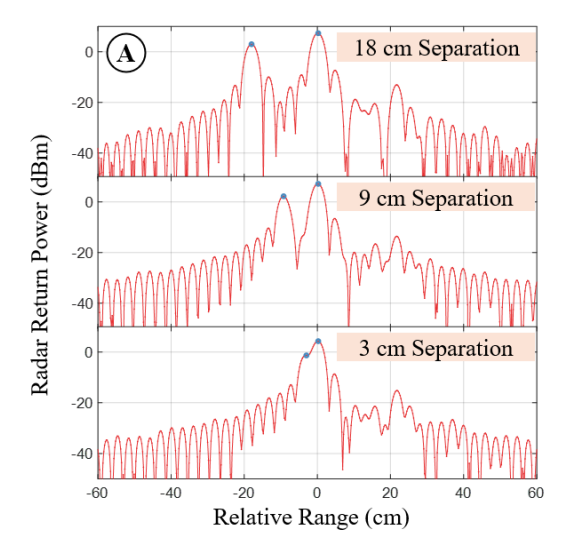


Fig. 3. A comparison of measured return SNR (data points connected by dotted lines) versus theoretical predictions (smooth, solid lines). The measured SNR saturates at approximately 48.5 dB, which is indicated by the dotted horizontal line on the plot. The two points on the -1.28 dBsm curve that significantly exceed the theoretical prediction are hypothesized to be caused by interference from spurious returns. The prediction and return SNR of the largest target are not shown.

The other discrepancy of note - namely, the slightly-too-small returns of the 24.6 dBsm target, are likely due to the increased multistatic loss inherent in higher-RCS (more directive) corner reflectors. Smaller TCRs have a less directive return signal, allowing proportionately more signal to couple into the receiver. On the other hand, larger TCRs will have higher multistatic loss; this, we believe, is causing the measured returns for the 24.6 dBsm TCR to be smaller than expected.

The results of the second suite of measurements, in which a pair of flat mirrors at 192.6 m were used to test range resolution, were also favorable. Fig 4(A) shows three representative outputs of the matched filter for plate separations of 18 cm, 9 cm, and 3 cm respectively, with

the range normalized to the return from the larger mirror. The separation of the two targets is clearly discernible in the 18 cm and 9 cm separation cases. In the 3 cm separation case, the two targets are nearly indistinguishable, due to the 3 cm range resolution of our system. Plate separations below this limit are not discernible, as predicted, and this is shown by the data points indicating a target separation of zero centimeters in Fig 4(B). Fig 4(B) also demonstrates the high ranging accuracy of the system (± 4 mm, and typically within ± 1 mm), as evidenced by the good linearity of the plot.



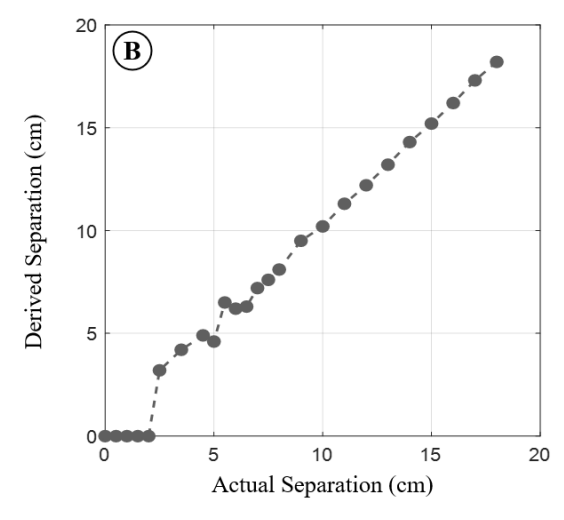


Fig. 4. (A) Matched filter output for two targets separated by 18 cm, 9 cm, and 3 cm, and (B) a comparison of calculated versus actual target separations. In (B), cases where the separation is zero indicate the radar could not resolve the individual targets. This occurs for target separations below the radar's range resolution of 30 mm.

V. DISCUSSION

Perhaps the most interesting result of these experiments is that the smallest TCR, which has an RCS somewhat below that of a small drone at 130 GHz, produced returns above the nominal 15 dB detection threshold at ranges exceeding 269 m. While our theoretical predictions indicate the smallest TCR would only be "detectable" out to 300 meters, these predictions are for a *single* sweep of only $2.5\,\mu s$. As described in the theoretical analysis above, the noise bandwidth of a radar system scales inversely with sweep time, meaning the SNR - and thus the average maximum detection range - can be increased by increasing the sweep time.

Alternatively (or additionally), multiple observations of the target can be averaged (or integrated) together to decrease the thermal noise power. If this integration is done coherently (i.e., if phase information is preserved, rather than averaging in intensity only) then the SNR will increase by a factor of M, where M is the number of observations taken. Thus, whether through repeated observation or extended sweep duration, the SNR will increase proportionally to the increase in total observation time.

Fig. 5 shows the relationship between observation time and average maximum detection range for our smallest TCR, and also for the lower and upper estimates for the RCS of a small-to-midsize drone (4.0 dBsm and 16.5 dBsm respectively). The maximum detection range rises very rapidly with increased observation time, but is ultimately limited by the increased atmospheric attenuation at longer distances. For the small TCR, the detection range exceeds 1 km within 1.5 ms, and at a standard "video quality" 60 Hz refresh rate (an observation time of 16.7 ms), the detection range is just over 1.5 km. For the highest RCS target, this 60 Hz refresh range could be up to 2.8 km. Distances exceeding a kilometer are sufficient enough to take meaningful action against a potentially hazardous inbound drone [1], thus, this experiment powerfully demonstrates the potential of terahertz radar to detect (and subsequently track) traditionally challenging low-RCS targets at appreciable distances, even in unfavorable atmospheric conditions (33 °C with 50% relative humidity).

Notably, our experiment (and previous discussion) was centered around single stationary targets in a relatively favorable environment. In reality, drones are dynamic targets and target-tracking schemes such as monopulse systems will be needed to keep them within the directive beams of terahertz-frequency systems. On the other hand, the highly directive beams employed by terahertz systems mean that the relatively clutter-free environment presented here is applicable to many real-life scenarios, and that individual targets can be tracked with high precision. As long as targets can be tracked reliably, the motion of targets will not fundamentally limit the attainable SNR except in cases where target moves so rapidly it exits the field of view before pulse integration is completed. In most cases, rotorcraft do not move at such high speeds.

Additionally, while the RCS of our targets matches the average RCS of commercial drones, real-life drones will present a fluctuating RCS, unlike the corner reflectors used in this experiment. However, RCS fluctuations are not unique to

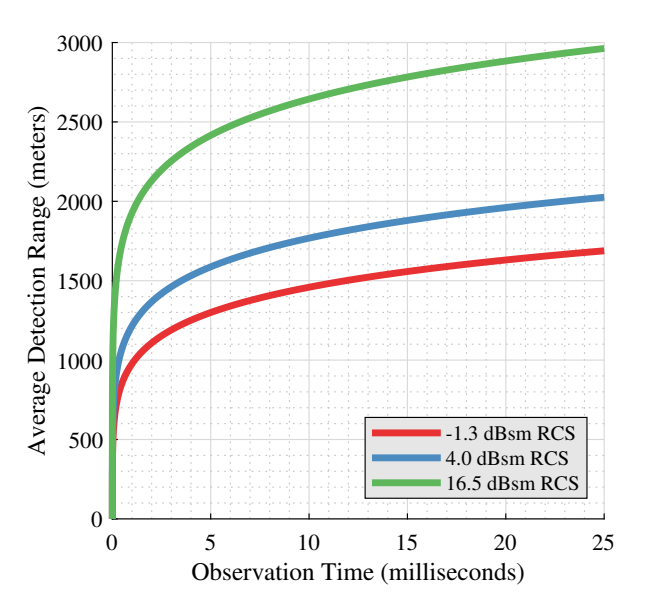


Fig. 5. A plot of average maximum detection range versus observation time for the TWISTER radar system, against targets with RCS values of −1.28 dBsm, 4.0 dBsm, and 16.5 dBsm at 130 GHz. This assumes a 15 dB detection threshold and, if multiple returns are averaged, that such averaging is done coherently. These results also assume a temperature of 33 °C with 50% relative humidity, which imposes a 2.5 dB/km penalty on both the outbound and return signal; this loss is accounted for in the curves plotted above.

terahertz frequencies and are reduced relative to microwave radars due to the greater diffuse scattering of the shorter wavelengths used above 100 GHz.

Finally, we wish to point out that a judicious application of spectrum shaping would clean up the ambiguity function of the radar signal, decreasing the interference between closely-spaced targets seen in Fig. 4(A). Our system employed a rectangular spectral amplitude weighting, which caused the slowly-decaying side lobes to appear on either side of true target features in the range domain. Ideal raised-cosine spectrum filtering would eliminate these side lobes, resulting in targets that rise sharply above the background noise. However, this would come at the cost of doubling the necessary sweep bandwidth (or, alternatively, degrading the range resolution by a factor of two for the same sweep bandwidth). Depending on the application, this might be an acceptable trade-off.

VI. CONCLUSION

The experimental results presented here demonstrate the potential of terahertz radar systems for detecting and identifying low-RCS targets, which have traditionally posed a challenge for detection systems. Through a series of mid-range (100 m scale) experiments, our general purpose TWISTER system was able to achieve sub-centimeter resolution and reliable detection of low RCS targets when configured as a FMCW radar. These results indicate that terahertz radars can overcome limitations faced by traditional detection systems,

such as sparse scattering by point targets, low micro-Doppler signatures, low range resolution, or blindness due to smoke, fog, etc. The high ranging resolution, combined with the ability to penetrate environmental obstructions, demonstrates the viability of terahertz radar for practical applications in security and defense. Future work will attempt to extend the observation time to increase the detection range, and utilize real-time signal processing implemented on an field programmable gate array to enable live detection and tracking of targets.

REFERENCES

- J. Farlik, M. Kratky, J. Casar, and V. Stary, "Radar cross section and detection of small unmanned aerial vehicles," in 2016 17th International Conference on Mechatronics-Mechatronika (ME). IEEE, 2016, pp. 1–7.
- [2] G. C. Birch and B. L. Woo, "Counter unmanned aerial systems testing: Evaluation of vis swir mwir and lwir passive imagers." Sandia National Lab.(SNL-NM), Albuquerque, NM (United States), Tech. Rep., 2017.
- [3] D. Heligman, Z. R. Spencer, and R. Mendis, "Terahertz imaging through fog," in *CLEO: Science and Innovations*. Optica Publishing Group, 2023, pp. JTh2A–108.
- [4] Z. R. Spencer, D. Heligman, and R. Mendis, "Terahertz imaging through dust," in *IEEE Research and Applications of Photonics in Defense (RAPID) Conference*. IEEE, 2024.
- [5] K. Su, L. Moeller, R. B. Barat, and J. F. Federici, "Experimental comparison of terahertz and infrared data signal attenuation in dust clouds," *JOSAA*, vol. 29, no. 11, pp. 2360–2366, 2012.
- [6] E. Marchetti, A. G. Stove, E. G. Hoare, M. Cherniakov, D. Blacknell, and M. Gashinova, "Space-based sub-thz isar for space situational awareness—concept and design," *IEEE Transactions on Aerospace and Electronic Systems*, vol. 58, no. 3, pp. 1558–1573, 2021.
- [7] E. Marchetti, A. G. Stove, E. G. Hoare, M. Cherniakov, D. Blacknell, and M. Gashinova, "Space-based sub-THz ISAR for space situational awareness Laboratory validation," *IEEE Transactions on Aerospace and Electronic Systems*, vol. 58, no. 5, pp. 4409–4422, 2022.
- [8] S. Rahman and D. A. Robertson, "Multiple drone classification using millimeter-wave cw radar micro-doppler data," in *Radar Sensor Technology XXIV*, vol. 11408. SPIE, 2020, pp. 50–57.
- [9] S. Rahman and D. A. Robertson, "Radar micro-doppler signatures of drones and birds at k-band and w-band," *Scientific reports*, vol. 8, no. 1, p. 17396, 2018.
- [10] V. Semkin, J. Haarla, T. Pairon, C. Slezak, S. Rangan, V. Viikari, and C. Oestges, "Analyzing radar cross section signatures of diverse drone models at mmwave frequencies," *IEEE access*, vol. 8, pp. 48958– 48969, 2020.
- [11] R. Nakamura, H. Hadama, and A. Kajiwara, "Ultra-wideband radar reflectivity of a drone in millimeter wave band," *IEICE Communications Express*, vol. 7, no. 9, pp. 341–346, 2018.
- [12] K. Strecker, W. Choi, and J. O'Hara, "A wideband millimeter-wave communication and sensing testbed for 75–500 GHz," in 2023 IEEE Texas Symposium on Wireless and Microwave Circuits and Systems (WMCS), 2023, pp. 1–5.
- [13] "Virginia Diodes, Inc," Available at http://www.vadiodes.com/en/ (2023/02/12).
- [14] A. W. Doerry, "Reflectors for sar performance testing," Sandia National Lab.(SNL-NM), Albuquerque, NM (United States), Tech. Rep., 2014
- [15] N. Levanon, Radar Principles. Wiley, 1988.